Precision Engineering 41 (2015) 119–125

Contents lists available at ScienceDirect

Precision Engineering

journal homepage: www.elsevier.com/locate/precision

Ion beam figuring machine for ultra-precision silicon spheres correction

Thomas Arnold*, Fred Pietag

Leibniz-Institut für Oberflächenmodifizierung (IOM), Permoserstr. 15, 04318 Leipzig, Germany

ARTICLE INFO

Article history:
Received 7 May 2014
Received in revised form
11 November 2014
Accepted 23 March 2015
Available online 31 March 2015

Keywords:
Ion beam figuring
Form error correction
Silicon sphere
Avogadro project

ABSTRACT

In the framework of the Avogadro project, isotopically enriched ^{28}Si spheres had been manufactured as artifacts for the assessment of various physical quantities including the sphere volume which finally leads to a very accurate determination of the Avogadro constant N_A. The Avogadro constant is an important input datum for the redefinition of the unit of mass, the kilogram, on the basis of fundamental physical constants. During the recent measurement campaign, it has turned out that one of the main contributions to the overall uncertainty of N_A is the sphericity error and consequently the interferometric volume measurement. Since chemical–mechanical polishing has reached its limits with respect to form accuracy due to the sensitivity of material removal rate to crystal orientation, it has been proposed to use ion beam figuring for further reduction of sphericity error from currently 50 nm PV to values <10 nm PV. In this paper, a new concept and realization of a multi-axis ion beam figuring machine dedicated for deterministic correction of silicon spheres is presented. Aspects of long term tool stability and alignment procedures in order to relate the ion beam footprint to the sphere surface are covered. Furthermore, a process dwell time calculation and tool path generation method dedicated for spheres manufacturing will be presented and discussed.

1. Introduction

Isotopically enriched ^{28}Si single crystal silicon spheres with nearly perfect spherical shape have been identified as suitable artifacts for volume and mass determination in the course of the accurate measurement of the Avogadro constant N_A [1]. The Avogadro constant is an important input datum for the redefinition of the unit of mass, the kilogram, on the basis of fundamental physical constants. Since 2005 the Avogadro project aims at ultimate measurement accuracy of the physical quantities that are required for the determination of N_A [2]. During the recent measurement campaign in 2011, it has turned out that one of the main contributions to the overall uncertainty of N_A is the sphericity error and consequently the interferometric volume measurement [3]. Two of such spheres with diameter of approx. 93.7 mm and a mass of 1 kg have been fabricated so far. Final polishing has been recently conducted by PTB, Germany. The ultimate roundness achievable on such spheres depends mainly on the mechanics of the grinding and polishing process. It has turned out that crystal orientation finally determines the local material removal in polishing. Deviations from ideal roundness are in the order of 30–50 nm peak-to-valley. The sphere volume is determined by measuring diameters using a spherical Fizeau interferometer developed at PTB [4,5]. Those interferometer measurements contain systematic errors partly originating from retrace errors due to shape deviations of the sphere under test. Since the uncertainty of the volume measurement contributes to the overall measurement uncertainty of the Avogadro number u_{N_A} by nearly 60%, it is necessary to reduce the roundness error below 10 nm peak to valley in order to achieve the required relative uncertainty $u_{N_A} < 2 \times 10^{-8}$.

It has been shown in the past that ion beam figuring (IBF) is a technology capable to correct optical surfaces with very high accuracy and process convergence due to its low and thus well controllable local material removal. Nowadays, IBF processes are widely applied in manufacturing and finishing of ultra-precision optical elements [6–8]. Therefore, it has been proposed to use IBF process for further correction of residual surface topography errors on the Avogadro silicon spheres. Although IBF is one of the standard machining processes in Leibniz-Institute of Surface Modification (IOM), the main challenge of this task is the handling and deterministic machining of a body with such a high symmetry. Hence, new concepts for ion beam figuring of spheres are required. In this paper we present the newly developed IBF system. In particular, we discuss the aspects of stable tool operation, sphere

* Corresponding author. Tel.: +49 341 235 3120; fax: +49 341 235 2595.
E-mail address: thomas.arnold@iom-leipzig.de (T. Arnold).

http://dx.doi.org/10.1016/j.precisioneng.2015.03.009

alignment procedures as well as processing data and tool path generation, which are important prerequisites for deterministic surface processing.

2. Ion beam figuring machine

Ion beam figuring is an established machining technique for ultra-precision optics fine correction on nanometer scale. It is based on physical sputtering of surface atoms by low energy ions (500–1000 eV) accelerated to the workpiece surface. Material removal rate depends on several physical parameters, e.g. ion mass, ion energy, ion incidence angle, and surface atom species. Usually, inert gases like argon are employed for ion beam sputtering. In order to ensure a mean free path long enough for generating and accelerating ions, a high vacuum environment is necessary. Together with NTG GmbH, a new IBF machine has been designed and built dedicated for spheres corrections. The system comprises three linear stages (*X*,*Y*,*Z*) and three rotary axes (*A*,*B*,*H*) for computer-controlled coordinated motion that are mounted in a high vacuum chamber with a volume of approx. 1 m^3. Fig. 1 shows a sketch of the motion system. The silicon sphere to be corrected rests on the table top of stage *A*, a direct driven rotary table that rotates the sphere around its vertical axis, which is designated as *z*-axis. In order to prevent any contamination or scratching of the surface, the sphere is supported by three pins made of polyether ether ketone (PEEK).

The ion beam source is mounted on the *Y*,*Z*,*B* stage group which allows to conduct meridional movements with respect to the sphere surface. With this configuration, every point of the upper hemisphere can be reached by the ion beam under normal incidence angle. Furthermore, a voice coil driven lifting mechanism together with a 3-point roller stage *H* can lift the sphere vertically by approx. 0.35 mm from its pin bearings on the A table. The sphere then rests on the horizontal rollers driven by motor *C* which can turn it over around the *y*-axis by 180° to make the lower hemisphere accessible (see also Fig. 4). After this rotation the lifting mechanism lowers the sphere again on its bearings on the A table for rotation about *z*-axis. The spindle-driven *X* stage serves for aligning the sphere in *x* direction and for positioning of the attached Faraday cup with respect to the ion beam.

The positioning errors of the rotational axes are specified to be lower than 5 arcsec. The orthogonality errors of the linear axes system are specified to be lower than 5 arcsec, i.e. less than 3–5 μm on travel ranges of 150 mm. None of the linear axis has specified positioning errors larger than 2.5 μm peak to valley. Thus, hitting a point at the sphere is secure within less than 15 μm in the worst case.

3. Ion beam source and ion beam diagnostics

The argon ion beam is generated by a standard 40 mm diameter radio-frequency (13.56 MHz) inductively coupled ion beam source equipped with a multi-grid system for beam extraction [9]. The grid system shields the plasma while allowing the positive ions to be transmitted into the free vacuum. High voltages applied to the outer grids lead to focusing of the beamlets resulting in a spatially constrained ion current density at a distance of approx. 40 mm off the outer grid position. An annular graphite aperture with 4 mm diameter at this position masks the beam further to create a nearly Gaussian shaped ion current density distribution with a full width at half maximum (FWHM) of similar order. In order to generate a quasi-neutral particle beam that is emitted by the source, a ring-shaped neutralizer hot filament is located in the gap between grid and graphite aperture for injecting electrons radially into the positive space charge of the ion beam. Beam neutralization is important to maintain stable sputtering conditions on electrically insulating substrates, e.g. made from glass or non-doped silicon. The ion beam source is equipped with an electrical beam switch that allows the switching of the beam quickly on and off [10]. This feature is necessary for start and stop of the machining procedure, since the ion beam source must be moved from its wait position to the start position and back to wait position with beam off to prevent uncoordinated surface treatment.

An ion beam current probe (Faraday cup) for in situ beam diagnostics is attached to the *X* stage parallel to the A table (see Figs. 1 and 4). With this probe the position of ion current density

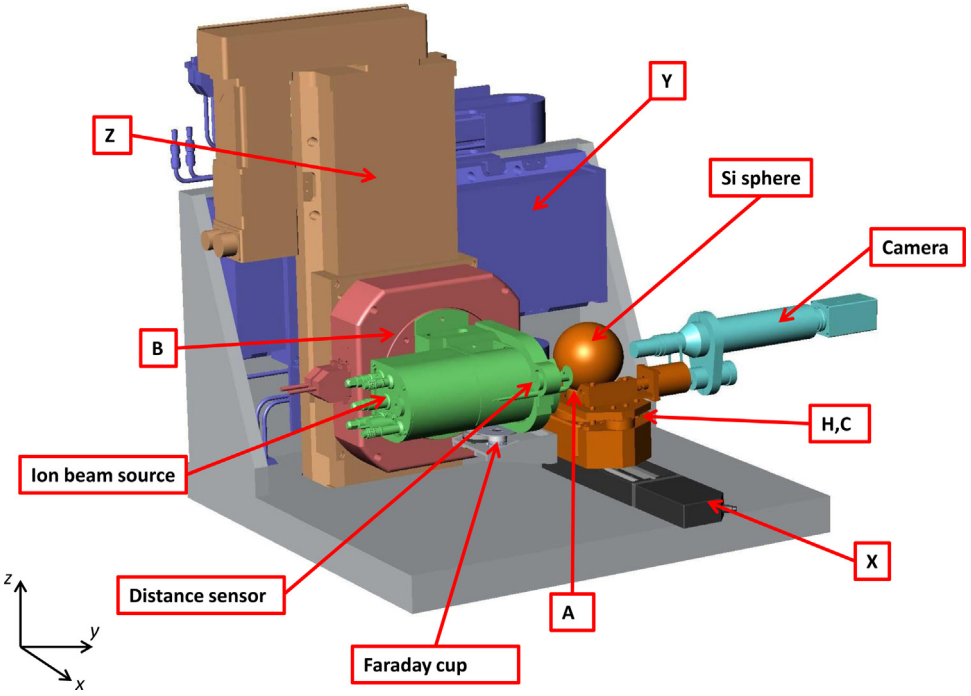

Fig. 1. IBF multi-axis motion system for Si sphere correction (courtesy of NTG GmbH, Gelnhausen, Germany).

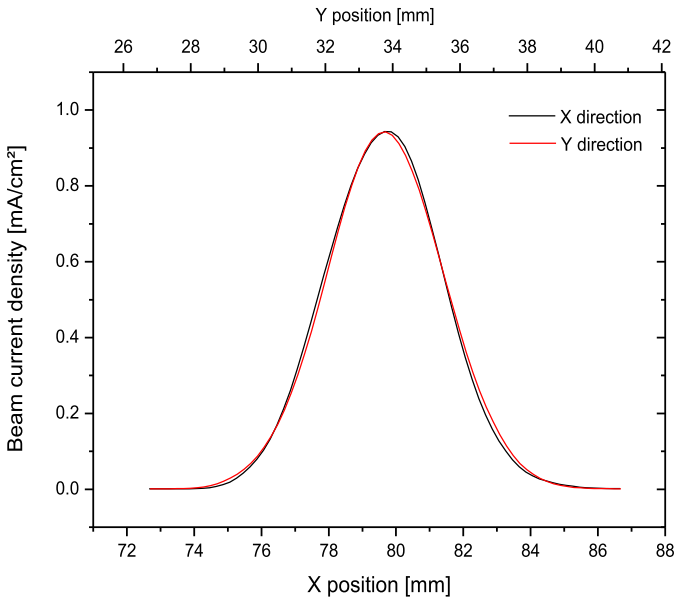

Fig. 2. Beam current density profiles in *X* and *Y* direction measured by Faraday cup.

distribution centroid is determined with respect to the machine coordinate system. Besides this, the approximate lateral beam shape and the maximum ion current density can be determined. Fig. 2 shows typical current density profiles in *x* and *y* direction obtained for a working distance between ion beam source and point of impact of 22 mm, revealing that the beam cross section can be described by a nearly rotationally symmetric Gaussian function. Since long term stability of the beam position and current density are essential for deterministic machining, beam centroid and maximum current density, respectively, have been recorded for a period of 7 h after switching on the ion beam source. During each beam current measurement the neutralizer has been temporarily switched off. The beam centroid positions and the maximum current density are shown in Fig. 3(a) and (b).

From both diagrams a distinct start-up phase lasting for approx. 100 min can be concluded. The centroid shifts by about 75 μm in *x* direction, while the *y* shift is less than 10 μm. This relatively large *x* shift can be mainly attributed to thermal expansion of the *X* stage, for the ion beam is representing a considerable thermal load and is dwelling over the Faraday cup during the full measurement time. The beam intensity falls by approx. 17% within the first 100 min.

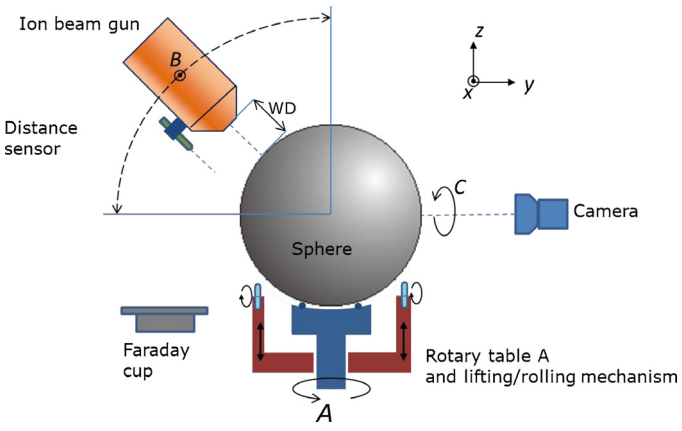

Fig. 4. Schematic setup of the alignment sensors and the main rotational axes. The *x* coordinate points out of the plane. WD indicates the working distance.

Thereafter, the beam conditions remain sufficiently stable. The current density varies within a range of 1.5%. The lateral shift of the centroid is less than ±7.5 μm.

As a consequence of these findings, beam centroid determination and subsequent ion beam processing of the silicon sphere should be started after 2 h start-up time. Furthermore, the beam should be directed to the free space in the vacuum chamber during the start-up phase to prevent heating of parts of the motion system and thermal relaxation later on during the sphere processing. Heating of the sphere itself during processing does not contribute to positioning errors since thermal expansion takes place more or less isotropically leading to a radius increase of approx. 20 μm for a temperature rise of 200 K. Accordingly, this expansion results in a slightly decreased working distance which can be neglected.

4. Silicon sphere alignment procedure and positioning uncertainty

The alignment sensor setup is schematically shown in Fig. 4. Alignment of the Si sphere relative to the ion beam figuring machine is done with the help of a confocal distance sensor mounted in parallel to the ion beam source on the *Y*, *Z*, *B* axis group. This sensor is used for position measurements of the sphere center point with respect to the Faraday cup as well as to the machine coordinate system. The sensor signal is synchronized with axis position data and has a measurement resolution of <60 nm. Furthermore, a high-resolution microscope camera is attached at the body of the *X*, *A*,

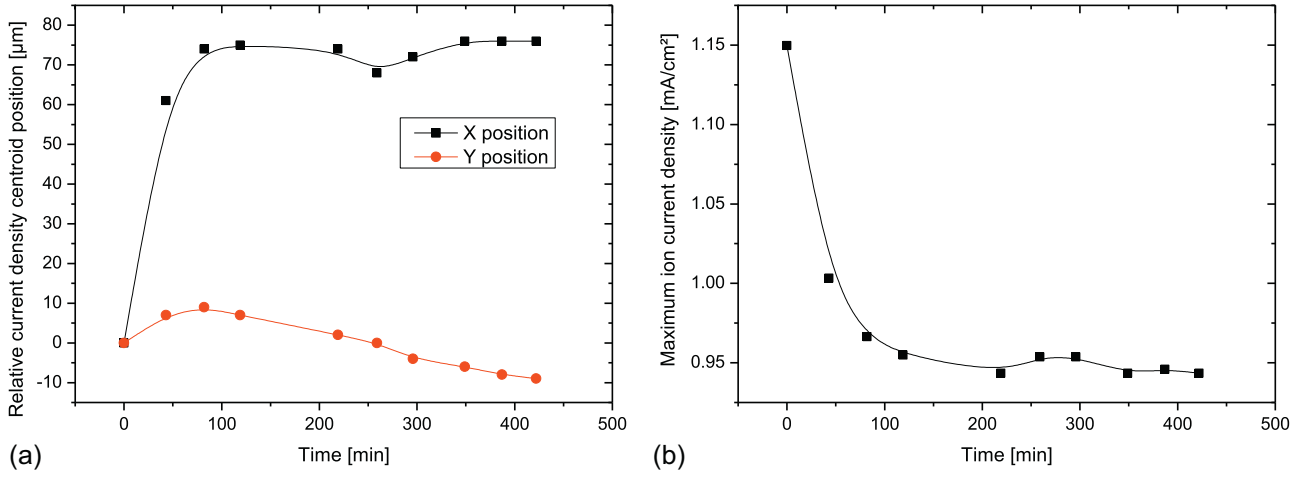

Fig. 3. (a) Lateral deviation of current density distribution centroid from initial position recorded over 7 h. (b) Maximum ion beam current density vs. time.

Table 1
Sources of position errors originating from motion system and sensors.

Error source	Meridional error [°]	Azimuthal error [°]
Motion system	±0.018	±0.018
Faraday cup position	±0.009	±0.009
Ion beam centroid	±0.012	±0.012
Sphere center point	±0.020	±0.010
Scratch mark distance sensor	±0.006	±0.006
Scratch mark camera	±0.012	±0.012
Fiducials imaging	±0.004	±0.004
Sum	±0.086	±0.076

H axis group opposite to the ion beam source position. The camera is directed to the sphere vertex in the equatorial plane. A camera resolution test has been performed by imaging a binary grating with a period of 200 μm. One pixel corresponds to 3.47 × 3.47 μm^2.

In practice, several error sources may occur which are connected to imaging and position measurement accuracy as well as the size and position measurement uncertainties of the fiducial marks which determine the reproducibility of sphere positioning. Measurements have been carried out in order to identify the main sources and to evaluate the contributions of positioning errors to the overall alignment accuracy.

The translational alignment of the sphere with respect to the machine coordinate system is done using the confocal sensor. The sphere center point is determined by areal scans of the sphere vertex regions in the *x*–*z* plane and in the *x*–*y* plane, respectively, and subsequent fitting the data by a spherical function. The uncertainty of the vertex position is ±6 μm in each direction. Additionally, the kinematic parameter for the ion beam source motion around this center point (i.e. the distance between sphere center point and rotational axis of B) is obtained with the same uncertainty of ±6 μm. A similar scan of the Faraday cup region is conducted to measure the center point of the electrode. The uncertainty of the measurement for *x* and *y* coordinate is ±10 μm.

For the rotational alignment of the silicon sphere the microscope camera is required, since the sphere is marked by laser written fiducial marks that are visible by an optical imaging system, only. Therefore, the geometric relation between the confocal sensor position and the camera image must be found. This is done by placing a thin scratch mark on a dummy sphere with the same dimensions as the silicon sphere in the vertex in the *x*–*z* plane. This mark can be detected by the confocal sensor with an uncertainty of ±10 μm, and subsequent imaging on the camera after rotation by 180° around the *z* axis. In this way the corresponding camera pixel determining the sphere vertex in the equatorial plane is identified with an uncertainty of ±10 μm. Fiducial marks attached on the sphere with known coordinates at two different positions can now be used for angular alignment. The mark positions have been determined by sphere interferometer measurements. The coordinate's uncertainties are ±0.1° or ±80 μm and ±0.6° or 500 μm, respectively. In principle, the alignment procedure is performed by an appropriate sequence of rotations around *z* and *y* axes, where the sphere must be lifted for motion by the C rollers. Finally, the positions of the fiducial marks are checked with the camera again. The fiducial mark positions can be resolved in vertical and horizontal direction (i.e. angles for rotation around *x* and *z* axes) with an uncertainty of ±7 μm.

In order to assess the contributions of the individual measurement uncertainties to the maximum position error of the tool with respect to the workpiece surface, the lateral shifts are calculated in terms of angular errors. Deviations in *x* direction contribute to azimuthal positioning errors, while deviations in *y* and *z* direction contribute to meridional errors. Table 1 summarizes the contributions of position measurement uncertainties originating from the motion system and the sensors. Table 2 lists the uncertainties in fiducial mark position determination.

Table 2
Sources of position errors due to uncertainty of fiducial mark positions attached on the sphere.

Error source	Meridional error [°]	Azimuthal error [°]
Fiducial 1 position	±0.100	±0.100
Fiducial 2 position	±0.600	±0.600
Sum	±0.700	±0.700

Obviously, the uncertainties of the fiducial mark positions on the Si sphere exceed the values of the machine related positioning errors. Thus, observing the corresponding arc lengths, the sphere can be aligned at best within ±0.63 mm for each direction. However, the alignment reproducibility is in the range of ±0.1° or ±70 μm.

During the machining process the sphere is rotated by table A. In order to maintain the sphere alignment at dynamic motion, the acceleration and deceleration limits, respectively, must be known to prevent slipping of the sphere on the PEEK pins, which would lead to azimuthal position errors. Several acceleration tests have been performed. Fig. 5 shows the maximum angular acceleration where no slipping of the sphere occurs. Obviously, the acceleration can be rather high for small velocities. The green marked range has been identified for secure motion of the sphere.

5. Deterministic figure correction

Deterministic correction means local removal of surface deviations from the nominal shape. This is done by a sub-aperture tool moving across the surface in maeander or spiral path. Deterministic correction techniques utilize the dwell time method, where the center point of the tool rests for a certain dwell time *t* on each surface position (*x*,*y*) depending on the measured local topography height error *h*(*x*,*y*) in order to remove material locally in the surrounding of (*x*,*y*). The general model equation

$$h(x, y) = R\left(x - x', y - y'\right) \times t\left(x', y'\right), \quad (1)$$

which determines the error height *h*(*x*,*y*) and denotes a convolution of the spatial material removal distribution, also referred to as tool function *R*(*x*,*y*), and the dwell times *t*(*x*,*y*). In order to obtain *t* for a given error topography, the reverse operation must be executed, which is done by sophisticated numerical de-convolution

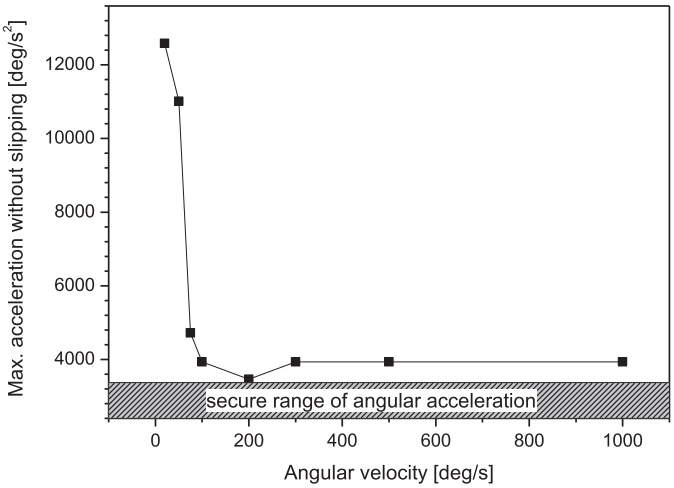

Fig. 5. Determination of secure range of acceleration for table A depending on angular velocity for the condition that no slipping of the sphere occurs.

algorithms developed for ion beam finishing of ultra-precision optics [11]. During the machining process material can only be removed. Possible re-deposition effects are not considered here. This assumption is equivalent to the side condition $t > 0$. Furthermore, those algorithms regard acceleration and velocity limits of the mechanical motion system to ensure a practical implementation on the ion beam figuring machine. This leads to an approximated solution of the deconvolution problem. From the resulting dwell time matrix a theoretical residual error map $e(x,y)$ is calculated for evaluation of the error correction capabilities under the given conditions. Generally, the theoretical residual error is largely determined by the relation between height error structure size and tool FWHM as well as by spatial resolution of the dwell time matrix.

Dwell time calculation is based on a sphere interferometer measurement performed at PTB. From the directly accessible diameter data the sphere radii are derived as a function of the spherical coordinates φ and θ [12]. The error topography h is obtained by subtraction of the mean radius. Fig. 6(a) shows a typical figure error in sinusoidal projection revealing relatively regular structures with peak-to-valley of 43 nm.

The tool function is obtained from ion beam test etchings of trenches performed with defined speed and number of repetitions. Fitting the trench profile shown in Fig. 6(b) yields parameters for an elliptical Gaussian function of the form

$$R(x,y) = A \exp\left\{ -\left(\frac{x^2}{\sigma_x^2} + \frac{y^2}{\sigma_y^2} \right) \right\}. \quad (2)$$

The FWHM of the tool function is nearly 3.5 mm.

De-convolution is done on a 2-D domain using spherical arc length coordinates ($r\varphi$, $r\theta$, h) as lateral coordinates. Spatial resolution (pixel size) of the radius data is 0.5 mm × 0.5 mm arc length. Other than an ordinary optical workpiece surface with distinct boundaries a sphere is a closed manifold without any boundaries, which makes it necessary to regard the continuity condition on the calculation domain edge. Thus, the de-convolution algorithm has been modified to meet this condition. Furthermore, the singular points on the polar positions as well as the pixels in the vicinity of the poles have been specially treated not to be met by the tool function center. In order to ensure the application of appropriate dwell times on these positions the dwell times of surrounding pixels that are explicitly met by the tool function center are adjusted by the algorithm.

Table 3
Results of dwell time calculation.

Parameter	Value (nm)
PV (initial)	43.29
PV (corrected)	3.87
RMS (initial)	7.95
RMS (corrected)	0.06
Base removal	0.976
Etching time in min	397

The results of the calculation are summarized in Table 3. Dwell time and theoretical residual error maps are shown in Fig. 7(a) and (b). Comparison of the RMS values before and after correction indicates that a theoretical error reduction by 75% can be achieved within 6 h 40 min machining time for the full sphere. The base removal is the minimal amount of material constantly removed over the whole surface. It is determined by the maximum velocity applicable to the motion system, and the line feed, respectively. The value for maximum velocity has been chosen in a way that the no-slip condition is satisfied.

In order to perform deterministic machining of a surface using, e.g., the dwell time method it is essential to align the surface properly with respect to the tool. Any deviation from perfect overlay between machine coordinate system and workpiece coordinates will contribute to machining errors. An estimation of alignment errors was given in the previous section. However, it can be shown that the sensitivity of this contribution depends largely on the mathematical description and especially on the lateral size of the tool function. It also depends on the spectral distribution of structure amplitudes of the error topography. The effect of misalignments in azimuthal direction has been investigated. Fig. 8(a) and (b) shows the parameters PV and RMS of the occurring residual errors $e(x,y)$ for the case where the dwell time data t are rotated relative to the height data h in azimuthal direction by a number N of measurement pixels with arc length of 0.5 mm (i.e. an angular misalignment of $N \times 0.01$ rad). The residual error map is obtained

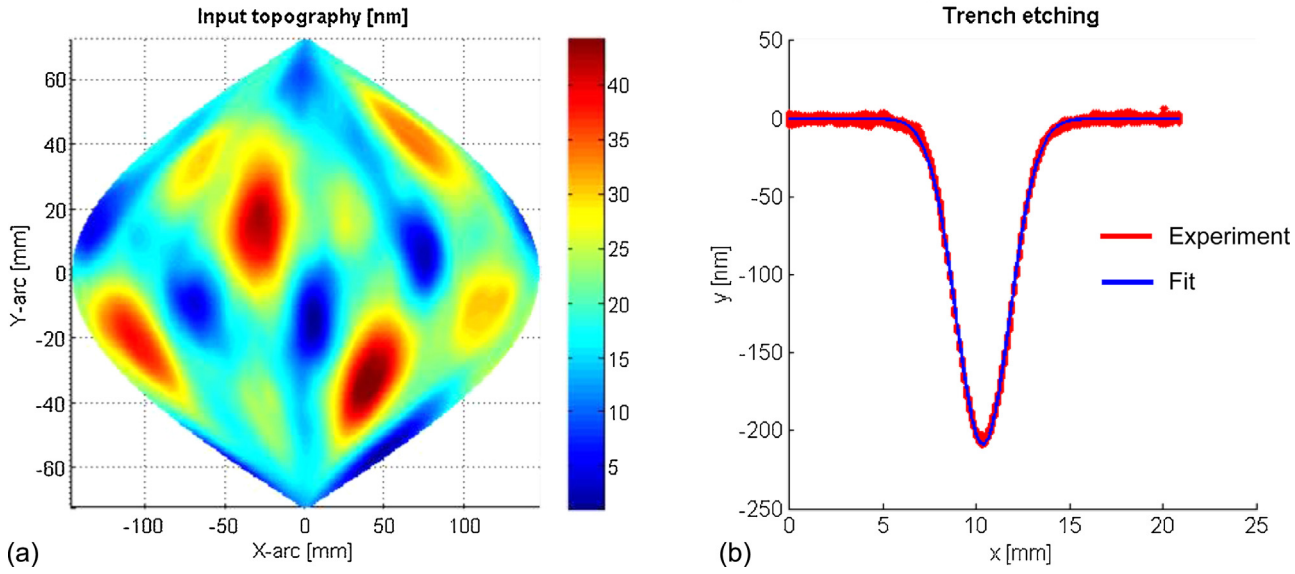

Fig. 6. (a) Surface figure error topography of a natural Si sphere in sinusoidal projection (PV 43 nm, RMS 7.95 nm). (b) Cross section of ion beam etched trench and Gaussian fit to obtain tool function parameters.

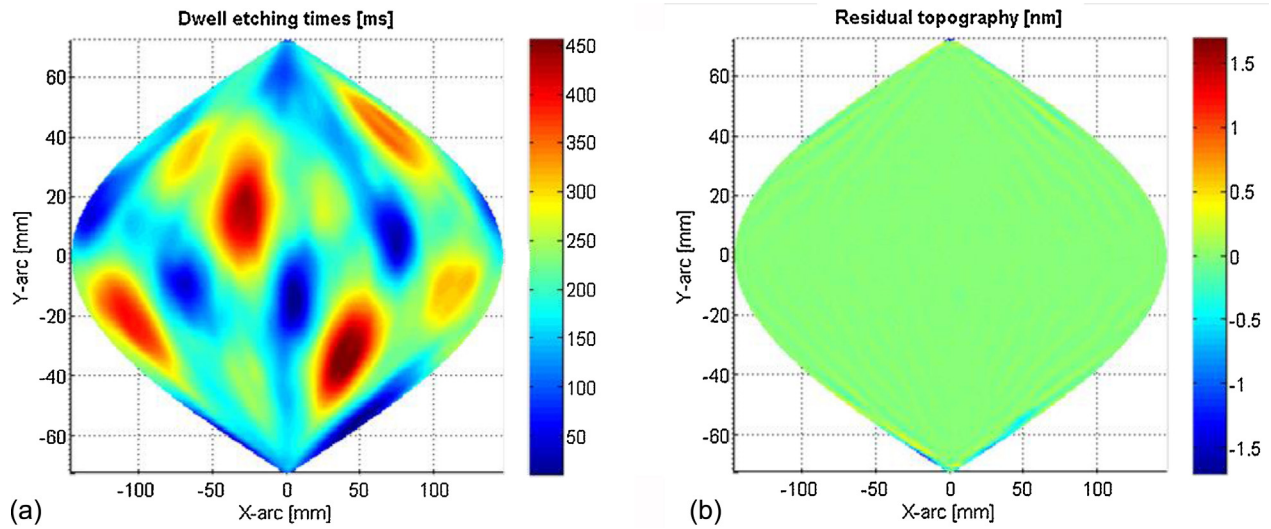

Fig. 7. (a) Calculated dwell time distribution and (b) theoretical residual topography error in sinusoidal projection.

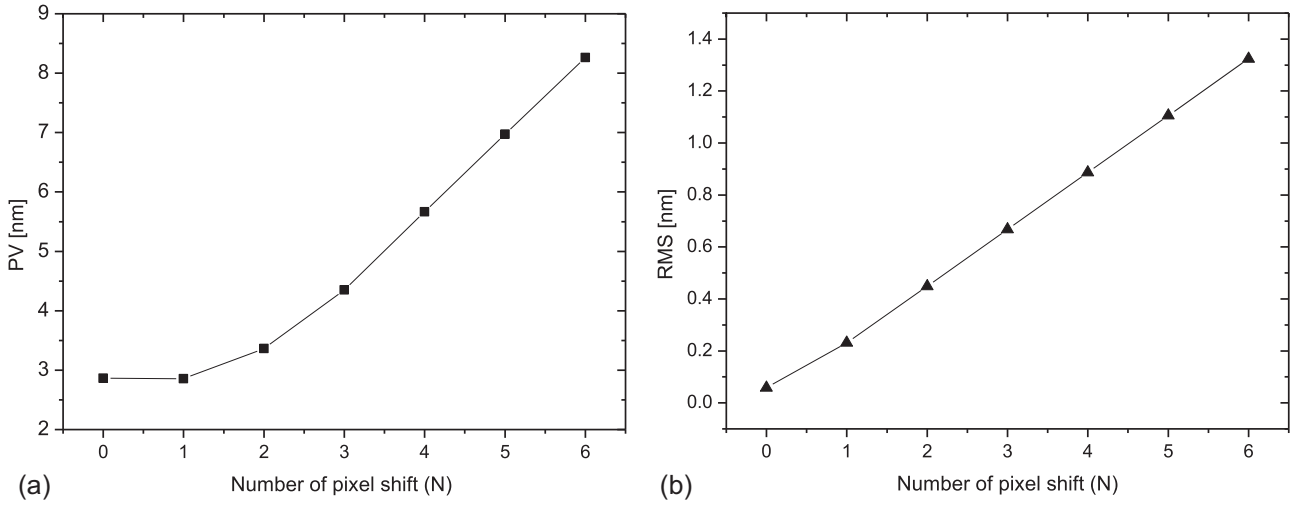

Fig. 8. Residual error in terms of (a) PV and (b) RMS values that occur if sphere alignment is rotated in azimuthal direction by N measurement pixels (i.e. shift of 1 pixel corresponds to an arc length of 0.5 mm or 0.01 rad).

via subtraction of h by the rotated data containing the calculated local material removal:

$$e(x,y) = h(x,y) - \left[R\left(x-x', y-y'\right) \times t\left(x'_{rot}, y'\right)\right]. \quad (3)$$

The diagrams show that even for several measurement pixels of rotational misalignment the theoretical residual error is still far below the required value of 10 nm PV. Thus, from the point of mechanical sphere alignment the requirements are somewhat relaxed. The estimated positioning error deduced from Tables 1 and 2 is still sufficient to achieve a surface topography within the required specification. In practice, additional errors like deviations from ideal Gaussian shape of the tool function, ion beam source degradation and current density fluctuations, or thermal expansion effects may contribute to the observable residual error after the machining procedure.

6. Tool path generation

A line-by-line raster tool path which is employed for 2-dimensional optical surface machining of lenses or mirrors that are bounded by a defined border is not applicable due to the spherical shape of the workpiece. The transition from one line to the next is usually performed by a line feed taking place outside the workpiece surface or at least outside the clear aperture. Since the ion beam takes effect on the material removal even for relatively large working distances the feed forward motion would be a rather undefined section of the dwell time controlled motion scheme. Furthermore, abrupt change of motion direction and velocity might stress the axis system and leads to possible slip of the sphere on its pin bearings and consequently to misalignment.

As an alternative, a tool path has been chosen that follows an Archimedean spiral with constant distance a between successive turns providing continuous line feed and preventing abrupt deceleration or acceleration of the motion axes. The spherical spiral path starting at the upper pole and ending at the lower pole is discretized by supporting points with an arc length b. Both a and b have been set to 0.5 mm providing an individual pixel area close to the pixel size used in the dwell time calculation. Hence, the sum of dwell times as well as their spatial distribution over the sphere surface is only minimally altered by 0.002% due to the transformation of the pixel from a matrix-like distribution to spiral distribution.

The motion velocity over an arc length is then determined by interpolation of the dwell time matrix and coded in G-code.

Since only the upper hemisphere is accessible in one step due to the axis configuration, the machining process starts on the equatorial position and ends in the vicinity of the pole. In order to prevent high rotational speeds and accelerations or decelerations at pole positions the pole itself is not covered. This corresponds to the calculated dwell time matrix where the pole and near-pole positions gain the appropriate dwell times from the surrounding pixels. Prior to the machining of the second hemisphere the Si sphere is lifted, turned upside down, put down on its bearings on the table A and checked for proper alignment again.

7. Conclusion

The paper describes a new concept for an ion beam figuring machine for figure error correction of Avogadro silicon spheres. Since deterministic surface correction requires

(a) Long term stability of the tool,
(b) Exact alignment of the workpiece with respect to the tool,
(c) De-convolution algorithm to calculate dwell times,
(d) Appropriate tool motion scheme relative to the workpiece surface,

each of the aspects have been investigated. It could be shown that the ion beam source can be operated in a stable regime after a ramp-up time of approx. 100 min. Furthermore, the position alignment of the sphere with respect to the machine coordinate system has been studied. Measurement uncertainty analysis revealed that position errors originating from the motion system or limited lateral resolution of sensors is of minor importance compared to the uncertainty of the fiducial mark positions on the sphere, which lie in the range of ± 0.7 mm.

Dwell time calculation methods dedicated for spherical surface machining have been developed. A theoretical study of the influence of lateral misalignment of the sphere with respect to the ion beam shows that a deviation of several measurement pixels of 0.5 mm arc length from ideal alignment retains the residual error well below the required 10 nm PV, provided that a Gaussian tool function with 3.5 mm FWHM is applied.

Finally, the paper describes a method to convert dwell time data into machining data, where the sphere is machined using a continuous spiral path rather than a line-by-line raster path.

With the knowledge gained during this work, the next step will be the performance of the complete ion beam figuring process using a well characterized natural silicon sphere.

Acknowledgements

The authors gratefully acknowledge valuable contributions by Thomas Franz (NTG GmbH) and Andreas Nickel (IOM).

Research in the framework of the Joint Research Programme SIB 03 – kNOW/REG1 was jointly funded by the European Metrology Research Programme (EMRP) participating countries within the European Association of National Metrology Institutes (EURAMET) and the European Union.

References

[1] Becker P, Friedrich H, Fujii K, Giardini W, Mana G, Picard A, et al. Meas Sci Technol 2009;20:092002.
[2] Becker und P, Gläser M. Int J Mass Spectrom 2006;251:220–30.
[3] Andreas B, Azuma Y, Bartl G, Becker P, Bettin H, Borys M, et al. Metrologia 2011;48:S1.
[4] Bartl G, Bettin H, Krystek M, Mai T, Nicolaus A, Peter A. Metrologia 2011;48:S96.
[5] Mai T, Bartl G, Nicolaus A. Conf Precis Electromagn Meas 2012:S474–5.
[6] Arnold T, Böhm G, Fechner R, Meister J, Nickel A, Frost F, et al. Nucl Instrum Methods Phys Res Sect Accel Spectrometers Detect Assoc Equip 2010;616:147–56.
[7] Weiser M. Nucl Instrum Methods Phys Res Sect B: Beam Interact Mater At 2009;267:1390–3.
[8] Gailly P. SPIE Newsroom 2008, http://dx.doi.org/10.1117/2.1200803.1106.
[9] Zeuner M, Scholze F, Dathe B, Neumann H. Surf Coat Technol 2001;142–144:39–48.
[10] Dienelt J, Zimmer K, Scholze F, Dathe B, Neumann H. Plasma Sources Sci Technol 2003;12:489.
[11] Hänsel T, Nickel A, Schindler A. OSA Technical Digest. USA: Rochester; 2008.
[12] Bartl G, Krystek M, Nicolaus A, Giardini W. Meas Sci Technol 2010;21:115101.